https://doi.org/10.5194/acp-2020-25
Preprint. Discussion started: 20 January 2020

Atmospheric Chemistry and Physics Discussions

Resonance-Enhanced Detection of Metals in Aerosols using Single Particle Mass Spectrometry

Johannes Passig[1,2,3], Julian Schade[2,3], Ellen Iva Rosewig[2,3], Robert Irsig[3,4], Thomas Kröger-Badge[2,3], Hendryk Czech[1,2,3], Martin Sklorz[1], Thorsten Streibel[1,2], Lei Li[5], Xue Li[5], Zhen Zhou[5], Henrik Fallgren[6], Jana Moldanova[6], and Ralf Zimmermann[1,2,3]

[1]Joint Mass Spectrometry Centre, Cooperation Group 'Comprehensive Molecular Analytics' (CMA), Helmholtz Zentrum München, 85764 Neuherberg, Germany
[2]Joint Mass Spectrometry Centre, Chair of Analytical Chemistry, University Rostock, 18059 Rostock, Germany
[3]Department Life, Light & Matter, University of Rostock, 18051 Rostock, Germany
[4]Photonion GmbH, 19061 Schwerin, Germany
[5]Institute of Mass Spectrometry and Atmospheric Environment, Jinan University, Guangzhou 510632, China and Guangzhou Hexin Instrument Co., LTD, Guangzhou 510530, China
[6]IVL Swedish Environmental Research Institute, 411 33 Gothenburg, Sweden

Correspondence to: Johannes Passig (johannes.passig@uni-rostock.de)

https://doi.org/10.5194/acp-2020-25
Preprint. Discussion started: 20 January 2020

Atmospheric Chemistry and Physics Discussions

Abstract. We describe resonance effects in laser desorption/ionization (LDI) of particles that substantially increase the sensitivity and selectivity to metals in single particle mass spectrometry (SPMS). Within the proposed scenario, resonant light absorption by ablated metal atoms increases their ionization rate within a single laser pulse. By choosing the appropriate laser wavelength, the key micronutrients Fe, Zn and Mn can be detected on individual aerosol particles with considerably improved efficiency. These ionization enhancements for metals apply to natural dust and anthropogenic aerosols, both important sources of bioavailable metals to marine environments. Transferring the results into applications, we show that the spectrum of our KrF-excimer laser is in resonance with a major absorption line of iron atoms. To estimate the impact of resonant LDI on the metal detection efficiency in SPMS applications, we performed a field experiment on ambient air with two alternately firing excimer lasers of different wavelengths. Herein, resonant LDI with the KrF-excimer laser (248.3 nm) revealed Fe signatures for many more aerosol particles compared to the more common ArF-excimer laser line of 193.3 nm. Moreover, resonant ionization of iron appeared to be less dependent on the particle matrix than conventional non-resonant LDI, allowing a more universal and secure detection of Fe. Our findings show a way to improve the detection and source attribution capabilities of SPMS for particle-bound metals, a health-relevant aerosol component and an important source of micronutrients to the surface oceans affecting marine primary productivity.

https://doi.org/10.5194/acp-2020-25
Preprint. Discussion started: 20 January 2020

Atmospheric Chemistry and Physics Discussions

1 Introduction

Natural and anthropogenic aerosols play a pivotal role in global climate and biogeochemical cycles, yet limited ambient observations result in large uncertainties. While sulfate and carbonaceous aerosols are intensively investigated for their climate effects (Bond et al., 2013; Kanakidou et al., 2005; Seinfeld and Pandis, 2016; Sofiev et al., 2018; Wang et al., 2016), the particle-bound metals have far-reaching impacts on ecosystems and human health. The redox cycling activity of inhaled transition metals such as iron (Fe) induces oxidative stress and is involved in severe health effects from air pollution (Fang et al., 2017; Oakes et al., 2012; Ye et al., 2018). Furthermore, atmospheric particles are important sources of marine micronutrients (Jickells et al., 2005; Mahowald et al., 2018). The highly soluble Fe from anthropogenic aerosols that adds to the larger flux of rather insoluble mineral dust is assumed to affect primary production and carbon export in a significant part of the world's oceans (Ito and Shi, 2016; Ito, 2015; Li et al., 2017). However, the magnitude and variability of this anthropogenic source of bioavailable metals in the sea are poorly characterized. Recently, anthropogenic fluxes and sources of Fe were estimated using isotope fingerprinting (Conway et al., 2019). Such studies require measurable differences between natural and anthropogenic isotope distributions of the respective metals. Alternative methods, preferably providing detailed source information, indicating the metals bioavailability and acquiring episodic deposition events are required to refine the global distribution models with observational data.

Several mass spectrometry based analytical techniques for aerosol characterization were developed, with single particle mass spectrometry (SPMS) being a real-time method obtaining the size and a chemical profile from individual particles (Laskin et al., 2018; Pratt and Prather, 2012). Herein, the particles are introduced into a vacuum, individually sized and exposed to intense UV laser pulses that form a partly ionized plume (laser desorption/ionization, LDI) (Hinz and Spengler, 2007; Murphy, 2007). Both positive and negative ions are extracted and analyzed with respect to their mass-to-charge ratio (m/z). Typical ionization products are e.g. organic fragments, salts, ammonia, nitrate, sulfate and carbon clusters from elemental or organic carbon (EC, OC). Beyond the single-particle aspect, SPMS stands out for its metal detection capabilities that yield unique source information data (Arndt et al., 2017; Dall'Osto et al., 2016a; Dall'Osto et al., 2016b; Pratt and Prather, 2012). However, compound-specific ionization efficiencies differ significantly. For example, the particle's humidity and its main components can have a strong effect on the detection of minor compounds (Neubauer et al., 1998), known as matrix effects. Several poorly determined interactions at the particle surface and in the desorbed plume affect ion formation (Hatch et al., 2014; Hinz and Spengler, 2007; Murphy, 2007; Reilly et al., 2000; Reinard and Johnston, 2008; Schoolcraft et al., 2000; Wade et al., 2008), reduce detection efficiencies and complicate quantification approaches (Fergenson et al., 2001; Gemayel et al., 2017; Gross et al., 2000; Healy et al., 2013; Qin et al., 2006; Shen et al., 2019; Zhou et al., 2016). These difficulties can be mitigated if the desorption and ionization are separated in a two-step process, and ions are formed by resonant ionization in the gaseous plume, as demonstrated for aromatic hydrocarbons (Bente et al., 2008; Morrical et al., 1998; Woods et al., 2001). Herein, thermal or laser desorption is followed by Resonance-Enhanced Multiphoton Ionization (REMPI) of the aromatic molecules (Gunzer et al., 2019). The approach yields detailed mass spectra of the health-relevant

https://doi.org/10.5194/acp-2020-25
Preprint. Discussion started: 20 January 2020


Atmospheric Chemistry and Physics Discussions

polycyclic aromatic hydrocarbons (PAHs) - ubiquitous trace compounds of combustion particles (Bente et al., 2009; Li et al., 2019; Passig et al., 2017; Schade et al., 2019). Resonant laser ablation of metals, where the leading edge of the laser pulse ablates atoms from a solid sample that are then ionized by the same pulse, have been studied some time ago for Laser Microprobe Mass Analysis (LAMMA) from surfaces (McLean et al., 1990; Verdun et al., 1987). However, to our best knowledge, such effects have so far not been recognized and applied in aerosol/single particle mass spectrometry. In the current study, we report on such wavelength-dependent enhancements in LDI ion yields of transition metals from aerosol particles. Using an optical parametric oscillator (OPO), we demonstrate that besides Fe, also the sparsely detected and biologically relevant trace metals Zn and Mn can be observed in anthropogenic particles with much higher sensitivity. We show that the resonant absorption of iron coincides with the spectrum of the field-deployable KrF-excimer laser and with the REMPI absorption spectra of most aromatic molecules. Thus, the enhanced detection sensitivity for metals can be combined with detailed spectra of aromatic substances via REMPI (Schade et al., 2019). This is of importance for health-related studies, as two of the most relevant adverse aerosol compounds, transition metals and PAHs, can be addressed with the same, easily accessible excimer laser wavelength. Finally, we demonstrate the application potential of the resonance effects in a field study comparing the KrF-excimer laser with a commonly used ArF-excimer laser for their Fe detection capabilities in ambient aerosols.

2 Experimental Section

The basic SPMS-instrument (Hexin Instruments Ltd., Guangzhou, P.R. China and Photonion GmbH, Schwerin, Germany) is described in other publications (Li et al., 2011). We equipped it with both a tuneable laser system (optical parametric oscillator, OPO) and excimer lasers (λ=248 nm and λ=193 nm) and replaced the Nd:YAG solid-state laser (λ=266 nm, 4th harmonic frequency) that belongs to the instruments standard configuration. Apart from the wavelength, most beam parameters were comparable throughout the experiments, see Table 1 for details. The pulse energy was measured at the optical entrance and exit of the mass spectrometer and the position of the focal lens (f=200 mm) was adjusted to maintain a comparable spot area, respective intensity for all wavelength comparison experiments. The OPO wavelengths as well as the KrF-excimer laser spectrum were measured with a LRL-005 spectrometer (MK Photonics Inc. U.S.). In the laboratory experiments, only particles with both a meaningful positive and negative ion spectrum were considered. Raw time-of-flight data was converted to mass spectra considering peak area within nominal mass resolution by custom software on Matlab platform (MathWorks Inc.).

Diesel exhaust particles from an old van (Volkswagen Transporter 1.7 D, build 1988) were collected from the inner surface of the exhaust tube. These particles exhibit a rather uniform chemical composition as demonstrated in previous experiments (Passig et al., 2017; Schade et al., 2019). Model particles for mineral dust were Arizona test dust 0-3 µm (Powder Technology Inc., U.S.) and complex anthropogenic aerosols with trace metals were modelled using NIST urban dust 1649b. Using a turntable-based powder disperser (Model 3433, TSI Inc., U.S.), particles were introduced into a 1 l/min carrier gas stream (N_2, purity: 5.0) from which 0.1 l/min were guided in an isokinetic flow into the instrument. For the experiments on

https://doi.org/10.5194/acp-2020-25
Preprint. Discussion started: 20 January 2020

Atmospheric Chemistry and Physics Discussions

ambient air, the SPMS instrument was set up at a meteorological station in a rural environment at the Swedish west coast, about 30 km south of Gothenburg (coordinates 57°23'37.8"N, 11°54'51.4"E). Ambient air was sampled at a height of 7 m above ground (15 m above sea level). Aerosols from a 300 l/min intake airflow were concentrated into the 1 l/min carrier gas stream using a first virtual impactor device (Model 4240, MSP corp., U.S.). After passing a dryer (Model MD-700-12S-1, Perma Pure LLC, U.S.), they were further concentrated to 0.1 l/min in a second step directly at the SPMS aerodynamic lens inlet. The two KrF and ArF excimer lasers used in this experiment were alternately triggered to particles using a custom electronic circuit and their beams were focused from opposite sides onto the particle beam, see Table 1 and section 3.3 for details.

Table 1. Light sources and details of the optical setup.

Laser source	Opolette HE 355 LD UV, Opotek LLC, U.S.	PhotonEx, Photonion GmbH, Germany	ATLEX-I 300, ATL GmbH, Germany
Laser medium	Optical Parametric Oscillator, Nd:YAG pumped	KrF gas (excimer)	ArF gas (excimer)
Wavelength (nm), photon energy (eV)	tuneable 210…2400	248, 4.99	193, 6.41
Pulse duration (ns)	≈5		
Beam size (mm)	Ø3 nearly Gaussian	3x6 Gaussian x flat top	3x6 Gaussian x flat top
Interaction spot distance to focus (mm)	≈8…11	7	7
Rayleigh length (mm)	≈1.2…1.5	1.4	1.1
Interaction spot size (µm)	Ø160	105x210	105x210
Pulse energy (mJ)	0.4	3	
Pulse intensity at interaction spot (GW/cm^2)	0.8	5	

3 Results and discussion

3.1 Resonance enhancements of Fe signals

We measured the Fe signals from diesel soot and Arizona desert dust particles as representative models of relevant anthropogenic and natural aerosols transporting Fe into the oceans. Figure 1 (a) and (b) show the respective mass spectra of positive and negative ions from LDI with two different wavelengths using the OPO. The mass spectra were accumulated over each 400 particles, without normalization or further processing. The observed peak broadening results mainly from averaging over single particle spectra with varying ion energy and starting positions. Typical signatures for (diesel) engine emissions (Toner et al., 2006) are recognizable, e.g. clusters of elemental carbon (EC, from soot) and organic hydrocarbon fragments (OC) (Silva and Prather, 2000). Also alkali metals are frequently detected due to their low ionization energy. The

https://doi.org/10.5194/acp-2020-25
Preprint. Discussion started: 20 January 2020

Atmospheric Chemistry and Physics Discussions

130 desert dust particles (Fig. 1b)) reveal typical mineral dust signals from metals and metal oxides (Sullivan et al., 2007; Dall'Osto et al., 2010). The slightly different laser wavelengths yield rather similar mass spectra, apart from some fragmentation differences for the soot particles in Fig. 1(a). However, much stronger Fe-signals can be observed for 248.3 nm for both particle types (see insets in Fig. 1(a) and (b)). This wavelength matches the $3d^64s^2 \rightarrow 3d^64s4p$ transition of Fe atoms, a line that is also typically used for Fe determination in atomic absorption spectroscopy. As apparent from the 135 histogram plots in Figure 1 (c) and (d), the enhancement effect is not resulting from some especial Fe-rich particles. Instead, most particles show higher Fe-signals at the resonance wavelength and the fraction of particles without Fe-signals drops considerably. However, the high Fe-content of Arizona dust particles (≈4-7%) often leads to saturated signals on the single-particle level and interferences with CaO^+ reduce the signal differences at m/z=56. Therefore, the histograms show the signal of the ^{54}Fe isotope. A further resonance enhancement can be noticed for Lithium at 242.2 nm because of the $1s^22s \rightarrow 1s^27p$ 140 transition closed to this wavelength.

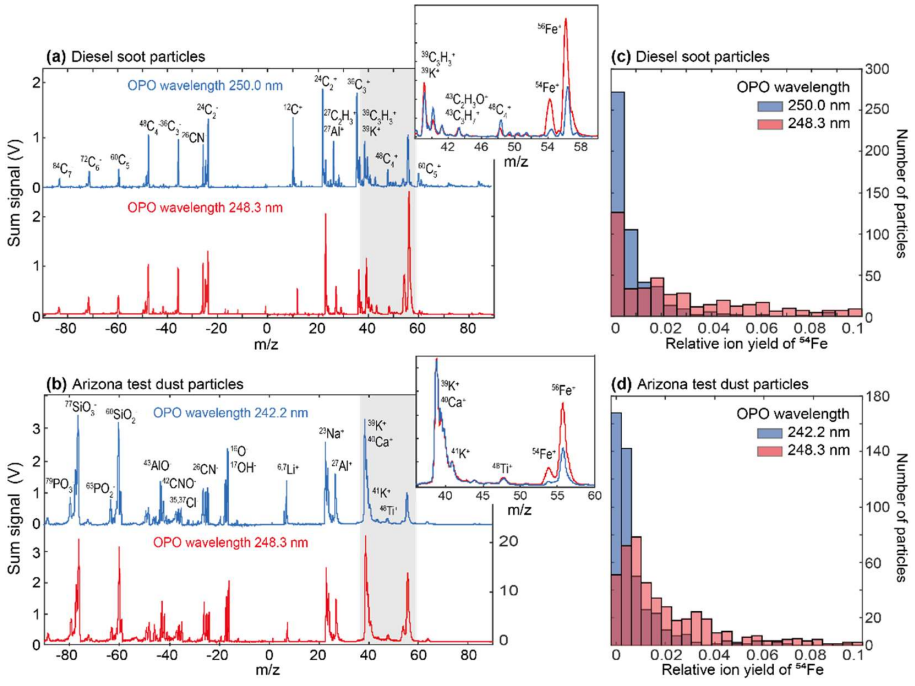

Figure 1: (a) Accumulated mass spectra (each n=400) of re-dispersed diesel soot particles ionized using the tuneable OPO laser. In the case of resonant ionization of Fe at 248.3 nm (red), the Fe signal is substantially enhanced compared to the non-resonant ionization at 250.0 nm (blue), see the inset for an enlarged view of the grey area. Most other signals are similar. (b) A comparable Fe-enhancement can 145 be observed for mineral dust particles. The histogram plots (c) and (d) of the single-particle relative ion signal ($^{54}Fe^+$ signal normalized to the particle's total ion yield) illustrate that the ionization enhancement accounts for the majority of analyzed particles. The particle size distributions are shown in Supplemental Fig. S4.

https://doi.org/10.5194/acp-2020-25
Preprint. Discussion started: 20 January 2020

Atmospheric Chemistry and Physics Discussions

To further investigate the enhancement effects, we measured the wavelength-dependent total ion yield of ^{54}Fe from each 400 particles, exposed to OPO laser pulses of the same intensity. As shown in Figure 2, the maximum Fe-signal is achieved near the resonance, with an enhancement of about 4 for diesel soot and mineral dust particles. The ion yield curves have a remarkably width and are much broader than the atomic lines or the OPO-linewidth (4…6 cm^{-1}). The absorption spectrum of Fe-atoms (blue) represents data from the NIST atomic spectra library (Kramida and Ralchenko). Such signal enhancements at specific wavelengths were not reported in previous SPMS studies, apart from the aforementioned REMPI-techniques. Thomson et al. observed for different salts, that the threshold intensity for ion formation decreased with increasing absorbance of the bulk material (Thomson et al., 1997). Generally, more substances are ionized at higher photon energies and lower laser intensities are required, but these effects tend to saturate at higher laser intensities (Thomson et al., 1997; Murphy, 2007). Even in a study using two MALDI matrix materials absorbing at different wavelengths, Wade et al. found only minimum wavelength effects on ion yields but a stronger dependence on the intensity and particle size (Wade et al., 2008). However, these results are not conflicting with the Fe resonance we observed. Several studies indicate that above a minimum intensity, effects in the plume dominate the ionization yield rather than the absorbance of the particle itself (Carson et al., 1997; Wade et al., 2008; Reinard and Johnston, 2008). The resonance begins to take effect as soon as Fe atoms are formed and vaporized from the particle during the initial phase of the laser pulse.

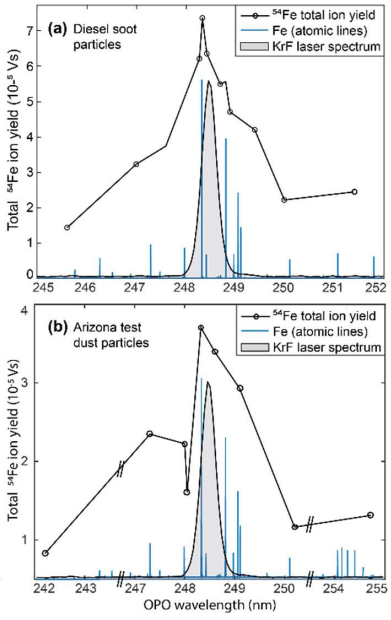

Figure 2: Wavelength-dependent total ion yield of ^{54}Fe in SPMS of re-dispersed particles (black circles, each n=400). Both for (a) diesel soot particles and (b) Arizona desert dust particles, the signal peaks for wavelengths that match a major atomic transition of Fe (blue lines). The large width of the curve is attributed to line broadening through interaction with the dense particle surface. Coincidentally, the Fe-lines are also addressed by our KrF-excimer laser (measured spectrum in grey). Atomic spectra from the NIST library (Kramida and Ralchenko). Mass spectra are shown in Figure 1 and size distributions in Supplemental Fig. S4.

https://doi.org/10.5194/acp-2020-25
Preprint. Discussion started: 20 January 2020


Atmospheric Chemistry and Physics Discussions

While so-far not recognized for SPMS, such resonance enhancements were previously reported and explained for laser ablation from solid surfaces. Using dye lasers, about five-fold signal increases were observed at the atomic lines of several metals and semiconductors (Verdun et al., 1987). The widths of the resonances were also rather broad, 0.4-0.7 nm. For low laser intensities, grazing incidence and two-step excitation, the width dropped below 0.05 nm (McLean et al., 1990) approaching the values of the respective atoms in gas phase ionization (Resonant Ionization MS, RIMS (Young et al., 1989)). The explanation for the broad signals in resonant ablation from surfaces and particles is rather simple: Broadening and transition wavelength shifts can be expected if the excitation happens when atoms are still bound in the matrix close to the surface (Verdun et al., 1987; McLean et al., 1990). Also the plasma pressure could contribute to these effects. With increasing time and distance from the dense target, the surface bonds vanish and the conditions become similar to RIMS. Minor contributions to the measured width could result from Stark broadening (typically at higher laser power (Hübert and Ankerhold, 2011)) and from interferences with the adjacent absorption lines.

3.2 Resonant Ionization of Trace Metals

Beyond Fe, further biologically important trace metals exert health effects (Gaur and Agnihotri, 2019) or can modulate primary production (Mahowald et al., 2018). For example, as enzyme co-factors they can determine which enzymes cells can express, affecting the composition of microbial communities (Boyd et al., 2017). Productivity-limiting deficiencies of e.g. manganese (Mn) and zinc (Zn) have been reported for marine regions (Mahowald et al., 2018). Zinc is also associated with toxicological responses to wood combustion aerosols (Uski et al., 2015; Kanashova et al., 2018). The resonant ionization of particle-bound Fe raises the question whether the SPMS-based detection of these metals may also benefit from the enhancement. We used NIST Reference Material Urban Dust 1649b (National Standard Institute of Technology – U.S.) as a well-characterized anthropogenic particle model containing several transition metals at low concentrations. Figure 3 shows accumulated cation mass spectra from resonant and non-resonant ionization with respect to strong atomic lines of Fe, Mn and Zn. The mass fraction of Fe is rather high (≈3%) and the signal enhancement at 248.3 nm (see Fig. 3(a)) corresponds to the results from diesel soot and Arizona dust. Manganese contributes a mass fraction of only 240 mg/kg to the dust. In general, for particles with organic content, the Mn signature at m/z=55 can hardly be distinguished from molecular fragments of the same mass. However, when the OPO wavelength is in resonance with the $3d^5 4s^2 \rightarrow 3d^5 4s4p$ transition of Mn at 279.5 nm, a clear signal appears at m/z=55, nearly as high as the peak of the much more abundant ^{56}Fe in the sum spectrum, see Fig. 3(b). Also for Zn (mass fraction 0.17%), there is a substantial difference and a clear signature appears in resonance case (Fig. 3(c)). Because the resonance wavelength of 213.8 nm is near the UV-limit of the OPO, the pulse energy of 0.25 mJ is lower than for the other metals. After resonant excitation at the respective wavelength, the absorption of a further single photon is sufficient for ionization of all three metals. The histogram plots (d…f) prove that not only the sum signals of the metals are higher in resonant case, but also more individual particles reveal their signatures. The results suggest that tuneable laser systems can be advantageous to enhance the detectability of various elements of interest in SPMS.

https://doi.org/10.5194/acp-2020-25
Preprint. Discussion started: 20 January 2020

Atmospheric Chemistry and Physics Discussions

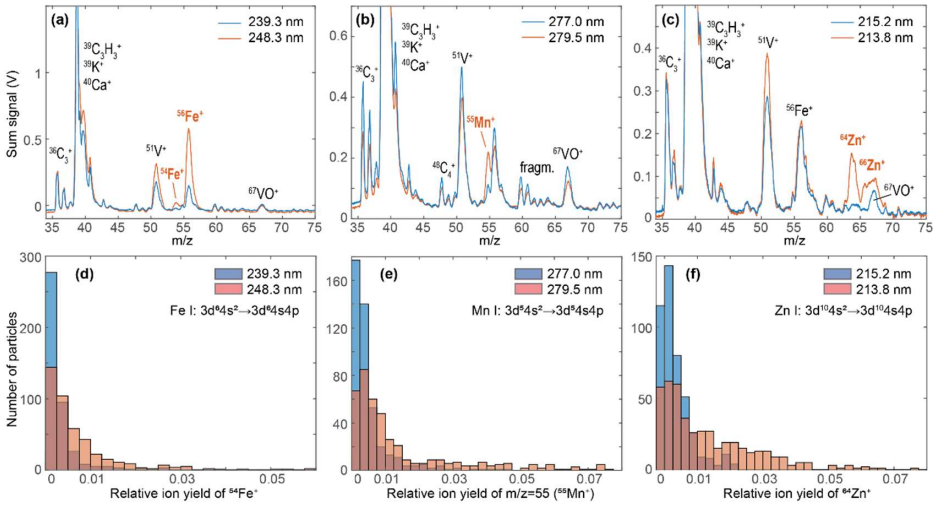

Figure 3: Accumulated cation mass spectra (n=400) of re-dispersed urban dust particles (Reference Material NIST 1649b). Using the tuneable OPO, the spectra were recorded at resonance wavelengths of each metal (red) and for the non-resonant case at a slightly different wavelength (blue). While carbon and molecular fragment signals are similar in the pairwise comparison, the resonant enhancements for (a) Fe, (b) Mn and (c) Zn are clearly visible. Complete, bipolar mass spectra and the size distribution are shown in Supplemental Fig. S1 and S4, respectively. (d-f) The single-particle distribution of the relative ion signals illustrates that the resonant ionization enhancement allows metal detection for many more particles. The respective resonance wavelengths (red) address the indicated transitions.

3.3 Application to long-range transported aerosols

While our laboratory experiments revealed remarkable resonance effects for several metals and particle types, these results have to be transferred into application on ambient aerosols. Tuneable laser systems are of limited suitability for field studies because of their complexity, low pulse power and repetition rate. In our experiments, thermal lensing problems of the irregularly triggered OPO system reduced its pulse power and stability. However, a freely triggerable OPO-SPMS with sufficient pulse energy is under development. In contrast to tuneable light sources, excimer lasers are cheaper, more robust and powerful. Of note, the KrF-excimer laser line at 248.3 nm coincidentally matches the strongest UV absorption line of Fe, a fact that gained little attention in the last decades (Trainor and Mani, 1978; Seder et al., 1986). The spectrum of our laser is shown in Fig. 2. We directly compare the Fe detection efficiencies of two field-deployable excimer lasers for the same ambient aerosol ensemble. The KrF-line is in resonance with the Fe absorption, while the often-used ArF-line is not. To exclude all effects from different instrumentation, both lasers are integrated into the same SPMS, firing with the same pulse parameters from opposite sites onto the particles, see Figure 4(a) and Table 1. A custom electronic circuit triggers the lasers alternately. With regard to the important application of detecting Fe-containing aerosols in remote regions, we designed our experiment to observe long-range transported anthropogenic particles with high secondary contributions in a marine environment. Therefore, we set up our instrument at the Swedish west coast and measured aerosols from central Europe after transport over the Baltic Sea, see the back-trajectories in Fig. 4(b).

https://doi.org/10.5194/acp-2020-25
Preprint. Discussion started: 20 January 2020

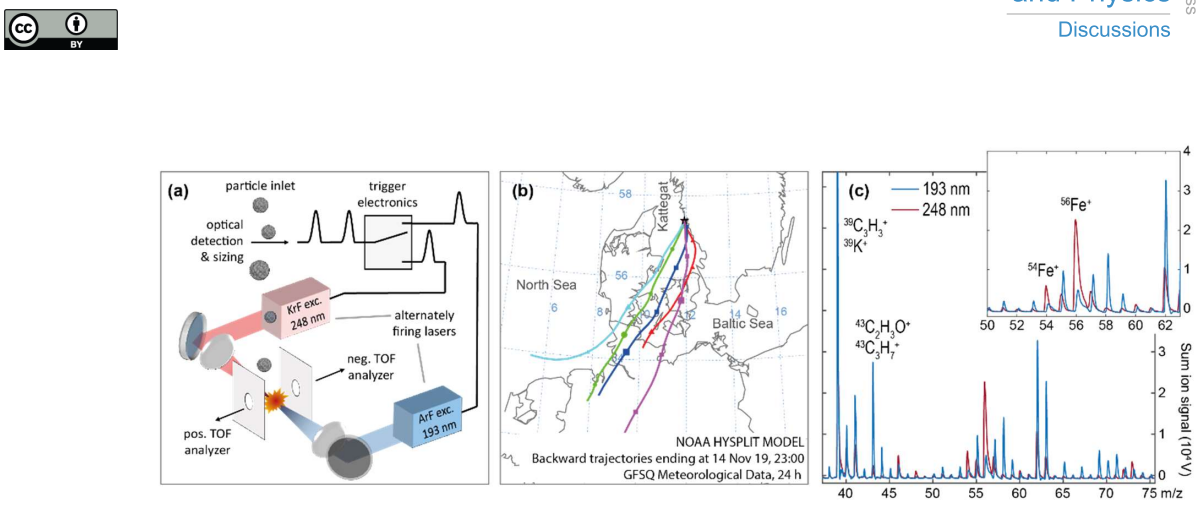

Figure 4: (a) Schematic view of the setup for direct comparison of non-resonant and resonant ionization of Fe in ambient air particles using the same mass spectrometer. The two lasers fired alternately on each 15,000 particles. (b) Back-trajectories from the HYSPLIT webtool (www.ready.noaa.gov/HYSPLIT.php), ending at the sampling site (sea level) during the experiment on long-range transported particles. (c) Accumulated cation mass spectra (each n=15,000) show a Fe^+-signal enhancement for ionization with the KrF excimer laser (248 nm, red) versus the ArF excimer laser (193 nm, blue). Further differences will be discussed in a different publication.

With each of the lasers, we analyzed 15,000 individual particles on the 14 November 2019 between 15:00 and 24:00 local time. Figure 4(c) shows the resulting sum mass spectra of cations for each ionization wavelength. The improved peak quality compared to Figs. 1 and 3 was achieved by implementing delayed ion extraction (Vera et al., 2005; Li et al., 2018). The enhanced Fe signature for the KrF-laser is clearly visible in the sum spectrum. All further wavelength-dependent differences will be discussed in a future publication. From each 15,000 particles exposed to the ArF-laser (KrF-laser), 13,776 (6,364) produced a negative spectrum, 12,217 (5,577) a positive signature and 12,189 (5,258) yielded bipolar mass spectra. The higher hit rate of the ArF laser results from the lower intensity thresholds for ion formation due to its higher photon energy (Thomson et al., 1997), thus yielding mass spectra also from particles that were not fully hit. Nearly all particles (>98 %) with negative spectra showed nitrate ($^{46}NO_2^-$ and $^{62}NO_3^-$). Because the steady onshore wind during the experiment excludes local sources of nitrate, these ions indicate condensation of NO_3 and replacement of Cl^- by NO_3^- (Gard et al., 1998; Arndt et al., 2017; Dall'Osto et al., 2016b) during long-range transport from central Europe (Dall'Osto et al., 2016a). Most single-particle spectra are dominated by either sea salt signatures ($^{23}Na^+$, $^{46}Na_2^+$, $^{62}Na_2O^+$, $^{63}Na_2OH^+$ and $^{81,83}Na_2Cl^+$) (Murphy et al., 2019), by organic fragments (e.g. $^{27}C_2H_3^+$, $^{39}C_3H_3^+$ and $^{39}K^+$, $^{43}C_2H_3O^+$ and $^{43}C_3H_7^+$) (Silva and Prather, 2000) or they reveal internal mixtures of these main components. To investigate the Fe-enhancements on the single-particle level and to analyze the role of the particle's main components, we performed a cluster analysis for each set of bipolar single-particle spectra, excluding the mass channels m/z=54…56 that bear potential Fe-signatures. We utilized the adaptive resonance theory neural network, ART-2a (Song et al., 1999) from the open-source toolkit FATES (Flexible Analysis Toolkit for the Exploration of SPMS data) (Sultana et al., 2017). With a learning rate 0.05, a vigilance factor of 0.8 and 20 iterations, the algorithm yielded 149 clusters for the particles ionized with the ArF-laser and 106 clusters for the KrF-laser ionization. Clusters with less than 20 particles were excluded from the analysis. Furthermore, clusters with comparable average mass spectra and the same major ions but slightly varying relative signal intensities were manually merged.

https://doi.org/10.5194/acp-2020-25
Preprint. Discussion started: 20 January 2020

Atmospheric Chemistry and Physics Discussions

Table 2. Main particle classes from ART-2a clustering and subsequent merging with respect to the major matrix components. The respective mass spectra are shown in Supplemental Figures S2 and S3.

	Aged sea salt	Aged sea salt & minor OC	Salt/OC mixed	OC	OC+EC	Fe	Anions only
Dominating ion signals	$^{23}Na^+$, $^{46}Na_2^+$ $^{62}Na_2O^+$, $^{63}Na_2OH^+$, $^{46}NO_2^-$, $^{62}NO_3^-$		$^{23}Na^+$, $^{46}Na_2^+$, $^{39}K^+$ & mol. fragments	$^{39}K^+$, $^{43}C_2H_3O^+$ & molecul. fragments, $^{18}NH_4^+$, $^{30}NO^+$, $^{59}C_3H_9N^+$ (TMA)		$^{56}Fe^+$, $^{73}FeOH^+$	$^{46}NO_2^-$, $^{62}NO_3^-$
Further required signals for assignment	$^{81,83}Na_2Cl^+$, $^{35,37}Cl^-$	$^{39}K^+$ & molecul. fragments	balanced ratio between salt & OC signatures	no or minimum salt signatures	$^{24}C_2^+$, $^{36}C_3^+$, $^{24}C_2^-$, $^{36}C_3^-$,		no cations

The particle ensemble revealed six dominating particle groups, as summarized in Table 2. The corresponding ART-2a area matrices representing the average intensity for each m/z and thus reflecting the typical mass spectra within a group are shown in Supplement Figures S2 and S3. Further separation into subgroups, e.g. with respect to signals from $^{18}NH_4^+$, $^{30}NO^+$ or trimethylamine (TMA, m/z=58…59) (Healy et al., 2015) had only limited effects on Fe detection and is consequently not shown here. Mineral dust particles were not observed in appreciable numbers. The measured size distribution is rather narrow, reflecting the instruments optimum detection efficiency that roughly coincides with the typical size mode undergoing long-range transport, see Supplemental Fig S5.

The particle numbers within the main classes are shown in Fig. 5. There are several differences between the two ionization wavelengths, e.g. the aforementioned overall hit rate. However, here we focus on the detection of Fe. In order to ensure a conservative effect registration (i.e. signals at m/z=56 may also stem from CaO^+ or molecular fragments like $C_3H_4O^+$) Fe-content is only accounted for particles with a peak area at m/z=56 that is larger than both the signals at m/z=40 (Ca^+) and m/z=55 (principal fragment signal). To further strengthen the screening as recommended by previous studies (Zhang et al., 2014; Dall'Osto et al., 2016a), particles with an additional signal at m/z=54 from the ^{54}Fe isotope, which is lower than 1/10 of the peak area of ^{56}Fe are represented by black bars. From the 15,000 particles exposed to the 193 nm laser pulses, less than 100 particles show Fe signatures according to this stringent criterion. As apparent from the enlarged view on the right of Fig. 5(a), nearly all these particles revealed also strong carbon cluster signals from EC. This suggests that they either belong to a particular Fe-rich aerosol class, e.g. from ship emissions or that the EC matrix augments the ionization process of Fe (Zimmermann et al., 2003) in contrast to a salt/OC-matrix, where energetically preferred ions survive collisional charge transfer in the plume (Reinard and Johnston, 2008). Also a suppression of specific ions by the presence of water is conceivable (Neubauer et al., 1998), although a dryer was applied in our experiment. A very different Fe-detection was achieved with the resonant ionization at 248 nm, see Fig. 5(b). Even though the total particle hit rate was lower, many more particles with Fe-signatures were detected. A key finding is that the Fe-detection is not limited to particles with EC-signatures anymore, but the Fe appears to be internally mixed within particles of several classes. (The relatively low abundance of Fe in the OC-class can be explained by the high contribution of wood/biomass combustion particles.) Remarkably, many particles with low cation signals reveal nearly exclusively Fe-signatures, providing an own group after further classification into subgroups (Fe-signatures were excluded from the first ART-2a clustering).

https://doi.org/10.5194/acp-2020-25
Preprint. Discussion started: 20 January 2020

Atmospheric Chemistry and Physics Discussions

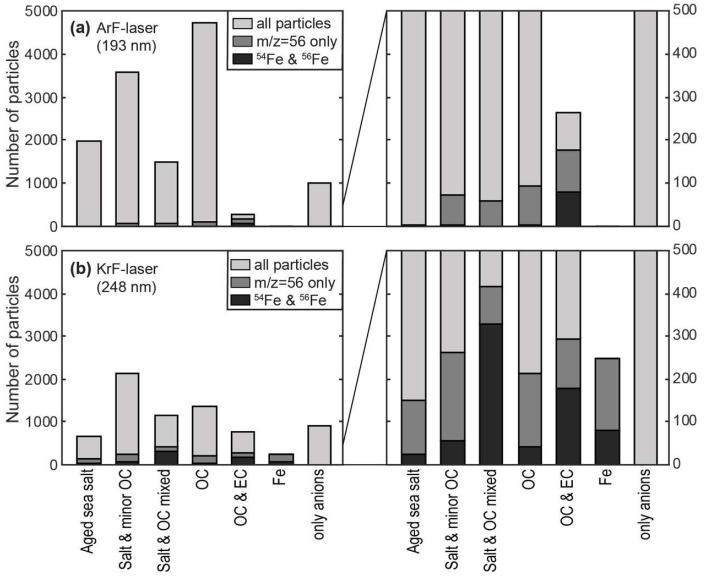

Figure 5. Number of particles within the main classes according to Table 2. Dark grey fractions represent particles with a peak area at m/z=56 being larger than at m/z=55 (molecular fragments) and m/z=40 (Ca^+, because of interference with $^{56}CaO^+$), indicating Fe content. Black fractions illustrate particles showing an additional signal of the less abundant isotope $^{54}Fe^+$. (a) If ionized with 193 nm pulses, substantial fragmentation leads to dominating fragment signals in many of the 15,000 exposed particles. Fe-signals are almost exclusively observed for particles with EC-signatures (see the enlarged view on the right), indicating a particularly high Fe-content or possible interactions with strongly absorbing soot during ionization. (b) Although fewer particles produce ion signals if exposed to 248 nm pulses, the particle fraction showing Fe-signatures is much larger and even a cluster with dominating Fe-signals appears. Of importance, the Fe-signals are not limited to EC-containing particles but can be observed for all classes. This suggests that the resonant ionization is less matrix-dependent and allows a more universal and secure detection of Fe.

Since the same aerosol ensemble was probed with both laser wavelengths, the appearance of Fe-signals for several particle matrices disagrees with the assumption of a particular Fe-rich class. In contrast, different ionization mechanisms are likely to determine the Fe-detection. This is in line with previous studies on REMPI of aromatic substances, showing that resonant ionization (of molecules) in the gaseous plume reduces matrix effects and improves quantification (Woods et al., 2001). Analogously, the reduced effect of the particle matrix renders resonant ionization at the appropriate wavelength a more universal ionization method for metals in SPMS.

4 Conclusions

In summary, we described enhancements in particle laser desorption/ionization that rely on resonant light absorption by metal atoms. Combining laboratory and field experiments, we showed that the mechanism can be exploited to improve the detection of relevant metals in both natural and anthropogenic aerosols on the single-particle level. The coincidental

https://doi.org/10.5194/acp-2020-25
Preprint. Discussion started: 20 January 2020


Atmospheric Chemistry and Physics Discussions

matching of the KrF laser line with a strong absorption of Fe atoms allows an easy and straightforward application of the resonance effect in the field. With the improved detection of Fe and its inherent sensitivity to further key nutrients such as nitrate and phosphate, SPMS becomes an interesting complement to established methods for investigating atmospheric Fe transport. Moreover, several key parameters for the metals bioavailability, including the particle size or the presence of carboxylic acids and sulfate can be determined on a single-particle level. Because of the high time resolution, SPMS-based Fe detection may be particularly helpful for studies on the oceans' rapid response to the naturally episodic depositions of Fe and other micronutrients. Beyond these direct applications, more studies are required to elucidate the promising implications for SPMS quantification approaches (Healy et al., 2013; Gemayel et al., 2017). Of note, the Fe-containing particles can further be characterized with regard to their organic content using multi-step ionization techniques (Schade et al., 2019; Czech et al., 2017). Such hyphenated single-particle schemes bear great potential to elucidate intriguing interactions in atmospheric heterogeneous and multiphase chemistry (Pöschl and Shiraiwa, 2015). In conclusion, the described resonance effects pave a new route towards improved detection of air pollutants and a more profound understanding of the aerosol impact on biogeochemical cycles and human health.

Data availability

Data are available on request from Johannes Passig (johannes.passig@uni-rostock.de).

Author Contributions

J.P. and J.S. contributed equally to this work. J.P. conceived the experiments. J.S., E.-I.R. J.P., T.K.-B. and R.I. performed the experiments. L.L., X.L. and Z.Z. provided the SPMS instrument as well as technical support. T.K.-B. developed the electronics. H.C., M.S., T.S. and R.Z. provided assistance with data interpretation. J.M. and H.F. hosted and supported the field study. J.S., J.P. and E.-I.R. analyzed data and prepared the figures. J.P. wrote the manuscript with contributions from all authors.

Competing interests

The authors declare that they have no conflict of interest.

Acknowledgements

We thank Johan Mellqvist, John Conway, Lars Eriksson and co-workers from the Chalmers University of Technology and from the IVL Miljöinstitut for hosting the field experiments and their support.

The Project was funded by the German Research Foundation (ZI 764/6-1), by the German Federal Ministry for Economic Affairs and Energy (ZF4402101 ZG7), by the Helmholtz International Lab aeroHEALTH (www.aerohealth.eu) and by the Helmholtz Virtual Institute of Complex Molecular Systems in Environmental Health (www.hice-vi.eu).

https://doi.org/10.5194/acp-2020-25
Preprint. Discussion started: 20 January 2020

Atmospheric Chemistry and Physics Discussions

References

Arndt, J., Sciare, J., Mallet, M., Roberts, G. C., Marchand, N., Sartelet, K., Sellegri, K., Dulac, F., Healy, R. M., and Wenger, J. C.: Sources and mixing state of summertime background aerosol in the north-western Mediterranean basin, Atmos. Chem. Phys., 17, 6975–7001, doi:10.5194/acp-17-6975-2017, 2017.

Bente, M., Sklorz, M., Streibel, T., and Zimmermann, R.: Online laser desorption-multiphoton postionization mass spectrometry of individual aerosol particles: molecular source indicators for particles emitted from different traffic-related and wood combustion sources, Anal. Chem., 80, 8991–9004, doi:10.1021/ac801295f, 2008.

Bente, M., Sklorz, M., Streibel, T., and Zimmermann, R.: Thermal desorption-multiphoton ionization time-of-flight mass spectrometry of individual aerosol particles: a simplified approach for online single-particle analysis of polycyclic aromatic hydrocarbons and their derivatives, Anal. Chem., 81, 2525–2536, doi:10.1021/ac802296f, 2009.

Bond, T. C., Doherty, S. J., Fahey, D. W., Forster, P. M., Berntsen, T., DeAngelo, B. J., Flanner, M. G., Ghan, S., Kärcher, B., Koch, D., Kinne, S., Kondo, Y., Quinn, P. K., Sarofim, M. C., Schultz, M. G., Schulz, M., Venkataraman, C., Zhang, H., Zhang, S., Bellouin, N., Guttikunda, S. K., Hopke, P. K., Jacobson, M. Z., Kaiser, J. W., Klimont, Z., Lohmann, U., Schwarz, J. P., Shindell, D., Storelvmo, T., Warren, S. G., and Zender, C. S.: Bounding the role of black carbon in the climate system: A scientific assessment, J. Geophys. Res., 118, 5380–5552, doi:10.1002/jgrd.50171, 2013.

Boyd, P. W., Ellwood, M. J., Tagliabue, A., and Twining, B. S.: Biotic and abiotic retention, recycling and remineralization of metals in the ocean, Nature Geosci, 10, 167–173, doi:10.1038/ngeo2876, 2017.

Carson, P. G., Johnston, M. V., and Wexler, A. S.: Real-Time Monitoring of the Surface and Total Composition of Aerosol Particles, Aerosol Sci. Technol., 26, 291–300, doi:10.1080/02786829708965431, 1997.

Conway, T. M., Hamilton, D. S., Shelley, R. U., Aguilar-Islas, A. M., Landing, W. M., Mahowald, N. M., and John, S. G.: Tracing and constraining anthropogenic aerosol iron fluxes to the North Atlantic Ocean using iron isotopes, Nat. Commun., 10, 1–10, doi:10.1038/s41467-019-10457-w, 2019.

Czech, H., Stengel, B., Adam, T., Sklorz, M., Streibel, T., and Zimmermann, R.: A chemometric investigation of aromatic emission profiles from a marine engine in comparison with residential wood combustion and road traffic: Implications for source apportionment inside and outside sulphur emission control areas, Atmospheric Environ., 167, 212–222, doi:10.1016/j.atmosenv.2017.08.022, 2017.

Dall'Osto, M., Harrison, R. M., Highwood, E. J., O'Dowd, C., Ceburnis, D., Querol, X., and Achterberg, E. P.: Variation of the mixing state of Saharan dust particles with atmospheric transport, Atmospheric Environ., 44, 3135–3146, doi:10.1016/j.atmosenv.2010.05.030, 2010.

https://doi.org/10.5194/acp-2020-25
Preprint. Discussion started: 20 January 2020

Dall'Osto, M., Beddows, D. C. S., Harrison, R. M., and Onat, B.: Fine Iron Aerosols Are Internally Mixed with Nitrate in the Urban European Atmosphere, Environ. Sci. Technol., 50, 4212–4220, doi:10.1021/acs.est.6b01127, 2016a.

Dall'Osto, M., Beddows, D. C. S., McGillicuddy, E. J., Esser-Gietl, J. K., Harrison, R. M., and Wenger, J. C.: On the simultaneous deployment of two single-particle mass spectrometers at an urban background and a roadside site during SAPUSS, Atmospheric Chemistry and Physics, 16, 9693–9710, doi:10.5194/acp-16-9693-2016, 2016b.

Fang, T., Guo, H., Zeng, L., Verma, V., Nenes, A., and Weber, R. J.: Highly Acidic Ambient Particles, Soluble Metals, and Oxidative Potential: A Link between Sulfate and Aerosol Toxicity, Environ. Sci. Technol., 51, 2611–2620, doi:10.1021/acs.est.6b06151, 2017.

Fergenson, D. P., Song, X. H., Ramadan, Z., Allen, J. O., Hughes, L. S., Cass, G. R., Hopke, P. K., and Prather, K. A.: Quantification of ATOFMS data by multivariate methods, Anal. Chem., 73, 3535–3541, doi:10.1021/ac010022j, 2001.

Gard, Kleeman, Gross, Hughes, Allen, Morrical, Fergenson, Dienes, E Galli, M., Johnson, Cass, and Prather: Direct observation of heterogeneous chemistry in the atmosphere, Science, 279, 1184–1187, doi:10.1126/science.279.5354.1184, 1998.

Gaur, S. and Agnihotri, R.: Health Effects of Trace Metals in Electronic Cigarette Aerosols-a Systematic Review, Biological trace element research, 188, 295–315, doi:10.1007/s12011-018-1423-x, 2019.

Gemayel, R., Temime-Roussel, B., Hayeck, N., Gandolfo, A., Hellebust, S., Gligorovski, S., and Wortham, H.: Development of an analytical methodology for obtaining quantitative mass concentrations from LAAP-ToF-MS measurements, Talanta, 174, 715–724, doi:10.1016/j.talanta.2017.06.050, 2017.

Gross, D. S., Gälli, M. E., Silva, P. J., and Prather, K. A.: Relative Sensitivity Factors for Alkali Metal and Ammonium Cations in Single-Particle Aerosol Time-of-Flight Mass Spectra, Anal. Chem., 72, 416–422, doi:10.1021/ac990434g, 2000.

Gunzer, F., Krüger, S., and Grotemeyer, J.: Photoionization and photofragmentation in mass spectrometry with visible and UV lasers, Mass Spectrom. Rev., 38, 202–217, doi:10.1002/mas.21579, 2019.

Hatch, L. E., Pratt, K. A., Huffman, J. A., Jimenez, J. L., and Prather, K. A.: Impacts of Aerosol Aging on Laser Desorption/Ionization in Single-Particle Mass Spectrometers, Aerosol Sci. Technol., 48, 1050–1058, doi:10.1080/02786826.2014.955907, 2014.

Healy, R. M., Evans, G. J., Murphy, M., Sierau, B., Arndt, J., McGillicuddy, E., O'Connor, I. P., Sodeau, J. R., and Wenger, J. C.: Single-particle speciation of alkylamines in ambient aerosol at five European sites, Analytical and bioanalytical chemistry, 407, 5899–5909, doi:10.1007/s00216-014-8092-1, 2015.

Healy, R. M., Sciare, J., Poulain, L., Crippa, M., Wiedensohler, A., Prévôt, A. S. H., Baltensperger, U., Sarda-Estève, R., McGuire, M. L., Jeong, C.-H., McGillicuddy, E., O&apos, Connor, I. P., Sodeau, J. R., Evans, G. J., and Wenger, J. C.: Quantitative determination of carbonaceous particle mixing state in Paris using single-particle mass spectrometer and aerosol mass spectrometer measurements, Atmos. Chem. Phys., 13, 9479–9496, doi:10.5194/acp-13-9479-2013, 2013.

https://doi.org/10.5194/acp-2020-25
Preprint. Discussion started: 20 January 2020

Hinz, K.-P. and Spengler, B.: Instrumentation, data evaluation and quantification in on-line aerosol mass spectrometry, Journal of mass spectrometry JMS, 42, 843–860, doi:10.1002/jms.1262, 2007.

Hübert, W. and Ankerhold, G.: Elemental misinterpretation in automated analysis of LIBS spectra, Analytical and bioanalytical chemistry, 400, 3273–3278, doi:10.1007/s00216-011-4793-x, 2011.

Ito, A.: Atmospheric Processing of Combustion Aerosols as a Source of Bioavailable Iron, Environ. Sci. Technol. Lett., 2, 70–75, doi:10.1021/acs.estlett.5b00007, 2015.

Ito, A. and Shi, Z.: Delivery of anthropogenic bioavailable iron from mineral dust and combustion aerosols to the ocean, Atmos. Chem. Phys., 16, 85–99, doi:10.5194/acp-16-85-2016, 2016.

Jickells, T. D., An, Z. S., Andersen, K. K., Baker, A. R., Bergametti, G., Brooks, N., Cao, J. J., Boyd, P. W., Duce, R. A., Hunter, K. A., Kawahata, H., Kubilay, N., laRoche, J., Liss, P. S., Mahowald, N., Prospero, J. M., Ridgwell, A. J., Tegen, I., and Torres, R.: Global iron connections between desert dust, ocean biogeochemistry, and climate, Science, 308, 67–71, doi:10.1126/science.1105959, 2005.

Kanakidou, M., Seinfeld, J. H., Pandis, S. N., Barnes, I., Dentener, F. J., Facchini, M. C., van Dingenen, R., Ervens, B., Nenes, A., Nielsen, C. J., Swietlicki, E., Putaud, J. P., Balkanski, Y., Fuzzi, S., Horth, J., Moortgat, G. K., Winterhalter, R., Myhre, C. E. L., Tsigaridis, K., Vignati, E., Stephanou, E. G., and Wilson, J.: Organic aerosol and global climate modelling: a review, Atmos. Chem. Phys., 5, 1053–1123, doi:10.5194/acp-5-1053-2005, 2005.

Kanashova, T., Sippula, O., Oeder, S., Streibel, T., Passig, J., Czech, H., Kaoma, T., Sapcariu, S. C., Dilger, M., Paur, H.-R., Schlager, C., Mülhopt, S., Weiss, C., Schmidt-Weber, C., Traidl-Hoffmann, C., Michalke, B., Krebs, T., Karg, E., Jakobi, G., Scholtes, S., Schnelle-Kreis, J., Sklorz, M., Orasche, J., Müller, L., Reda, A., Rüger, C., Neumann, A., Abbaszade, G., Radischat, C., Hiller, K., Grigonyte, J., Kortelainen, M., Kuuspalo, K., Lamberg, H., Leskinen, J., Nuutinen, I., Torvela, T., Tissari, J., Jalava, P., Kasurinen, S., Uski, O., Hirvonen, M.-R., Buters, J., Dittmar, G., Jokiniemi, J. K., and Zimmermann, R.: Emissions from a modern log wood masonry heater and wood pellet boiler Composition and biological impact on air-liquid interface exposed human lung cancer cells, Journal of Molecular and Clinical Medicine, 1, 23, doi:10.31083/j.jmcm.2018.01.004, 2018.

Kramida, A. and Ralchenko, Y.: NIST Atomic Spectra Database, NIST Standard Reference Database 78.

Laskin, J., Laskin, A., and Nizkorodov, S. A.: Mass Spectrometry Analysis in Atmospheric Chemistry, Anal. Chem., 90, 166–189, doi:10.1021/acs.analchem.7b04249, 2018.

Li, C., He, Q., Schade, J., Passig, J., Zimmermann, R., Meidan, D., Laskin, A., and Rudich, Y.: Dynamic changes in optical and chemical properties of tar ball aerosols by atmospheric photochemical aging, Atmos. Chem. Phys., 19, 139–163, doi:10.5194/acp-19-139-2019, 2019.

Li, L., Huang, Z., Dong, J., Li, M., Gao, W., Nian, H., Fu, Z., Zhang, G., Bi, X., Cheng, P., and Zhou, Z.: Real time bipolar time-of-flight mass spectrometer for analyzing single aerosol particles, Int. J. Mass Spectrom., 303, 118–124, doi:10.1016/j.ijms.2011.01.017, 2011.

https://doi.org/10.5194/acp-2020-25
Preprint. Discussion started: 20 January 2020

Li, L., Liu, L., Xu, L., Li, M., Li, X., Gao, W., Huang, Z., and Cheng, P.: Improvement in the Mass Resolution of Single Particle Mass Spectrometry Using Delayed Ion Extraction, J. Am. Soc. Mass Spectrom., 29, 2105–2109, doi:10.1007/s13361-018-2037-4, 2018.

Li, W., Xu, L., Liu, X., Zhang, J., Lin, Y., Yao, X., Gao, H., Zhang, D., Chen, J., Wang, W., Harrison, R. M., Zhang, X., Shao, L., Fu, P., Nenes, A., and Shi, Z.: Air pollution-aerosol interactions produce more bioavailable iron for ocean ecosystems, Sci. Adv., 3, e1601749, doi:10.1126/sciadv.1601749, 2017.

Mahowald, N. M., Hamilton, D. S., Mackey, K. R. M., Moore, J. K., Baker, A. R., Scanza, R. A., and Zhang, Y.: Aerosol trace metal leaching and impacts on marine microorganisms, Nat. Commun., 9, 2614, doi:10.1038/s41467-018-04970-7, 2018.

McLean, C. J., Marsh, J. H., Land, A. P., Clark, A., Jennings, R., Ledingham, K.W.D., McCombes, P. T., Marshall, A., Singhal, R. P., and Towrie, M.: Resonant laser ablation (RLA), Int. J. Mass Spectrom., 96, R1-R7, doi:10.1016/0168-1176(90)80047-7, 1990.

Morrical, B. D., Fergenson, D. P., and Prather, K. A.: Coupling two-step laser desorption/ionization with aerosol time-of-flight mass spectrometry for the analysis of individual organic particles, J. Am. Soc. Mass Spectrom., 9, 1068–1073, doi:10.1016/S1044-0305(98)00074-9, 1998.

Murphy, D. M.: The design of single particle laser mass spectrometers, Mass Spectrom. Rev., 26, 150–165, doi:10.1002/mas.20113, 2007.

Murphy, D. M., Froyd, K. D., Bian, H., Brock, C. A., Dibb, J. E., DiGangi, J. P., Diskin, G., Dollner, M., Kupc, A., Scheuer, E. M., Schill, G. P., Weinzierl, B., Williamson, C. J., and Yu, P.: The distribution of sea-salt aerosol in the global troposphere, Atmos. Chem. Phys., 19, 4093–4104, doi:10.5194/acp-19-4093-2019, 2019.

Neubauer, K. R., Johnston, M. V., and Wexler, A. S.: Humidity effects on the mass spectra of single aerosol particles, Atmospheric Environ., 32, 2521–2529, doi:10.1016/S1352-2310(98)00005-3, 1998.

Oakes, M., Ingall, E. D., Lai, B., Shafer, M. M., Hays, M. D., Liu, Z. G., Russell, A. G., and Weber, R. J.: Iron solubility related to particle sulfur content in source emission and ambient fine particles, Environ. Sci. Technol., 46, 6637–6644, doi:10.1021/es300701c, 2012.

Passig, J., Schade, J., Oster, M., Fuchs, M., Ehlert, S., Jäger, C., Sklorz, M., and Zimmermann, R.: Aerosol Mass Spectrometer for Simultaneous Detection of Polyaromatic Hydrocarbons and Inorganic Components from Individual Particles, Anal. Chem., 89, 6341–6345, doi:10.1021/acs.analchem.7b01207, 2017.

Pöschl, U. and Shiraiwa, M.: Multiphase chemistry at the atmosphere-biosphere interface influencing climate and public health in the anthropocene, Chem. Rev., 115, 4440–4475, doi:10.1021/cr500487s, 2015.

Pratt, K. A. and Prather, K. A.: Mass spectrometry of atmospheric aerosols--recent developments and applications. Part II: On-line mass spectrometry techniques, Mass Spectrom. Rev., 31, 17–48, doi:10.1002/mas.20330, 2012.

Qin, X., Bhave, P. V., and Prather, K. A.: Comparison of two methods for obtaining quantitative mass concentrations from aerosol time-of-flight mass spectrometry measurements, Anal. Chem., 78, 6169–6178, doi:10.1021/ac060395q, 2006.

https://doi.org/10.5194/acp-2020-25
Preprint. Discussion started: 20 January 2020

Reilly, P. T. A., Lazar, A. C., Gieray, R. A., Whitten, W. B., and Ramsey, J. M.: The Elucidation of Charge-Transfer-Induced Matrix Effects in Environmental Aerosols Via Real-Time Aerosol Mass Spectral Analysis of Individual Airborne Particles, Aerosol Sci. Technol., 33, 135–152, doi:10.1080/027868200410895, 2000.

Reinard, M. S. and Johnston, M. V.: Ion formation mechanism in laser desorption ionization of individual nanoparticles, J. Am. Soc. Mass Spectrom., 19, 389–399, doi:10.1016/j.jasms.2007.11.017, 2008.

Schade, J., Passig, J., Irsig, R., Ehlert, S., Sklorz, M., Adam, T., Li, C., Rudich, Y., and Zimmermann, R.: Spatially Shaped Laser Pulses for the Simultaneous Detection of Polycyclic Aromatic Hydrocarbons as well as Positive and Negative Inorganic Ions in Single Particle Mass Spectrometry, Anal. Chem., 91, 10282–10288, doi:10.1021/acs.analchem.9b02477, 2019.

Schoolcraft, T. A., Constable, G. S., Zhigilei, L. V., and Garrison, B. J.: Molecular dynamics simulation of the laser disintegration of aerosol particles, Anal. Chem., 72, 5143–5150, doi:10.1021/ac0007635, 2000.

Seder, T. A., Ouderkirk, A. J., and Weitz, E.: The wavelength dependence of excimer laser photolysis of Fe(CO) 5 in the gas phase. Transient infrared spectroscopy and kinetics of the Fe(CO) x (x =4,3,2) photofragments, J. Chem. Phys., 85, 1977–1986, doi:10.1063/1.451141, 1986.

Seinfeld, J. H. and Pandis, S. N.: Atmospheric chemistry and physics: From air pollution to climate change, 3rd edition, Wiley, Hoboken, New Jersey, 1120 pp., 2016.

Shen, X., Saathoff, H., Huang, W., Mohr, C., Ramisetty, R., and Leisner, T.: Understanding atmospheric aerosol particles with improved particle identification and quantification by single-particle mass spectrometry, Atmos. Meas. Tech., 12, 2219–2240, doi:10.5194/amt-12-2219-2019, 2019.

Silva, P. J. and Prather, K. A.: Interpretation of Mass Spectra from Organic Compounds in Aerosol Time-of-Flight Mass Spectrometry, Anal. Chem., 72, 3553–3562, doi:10.1021/ac9910132, 2000.

Sofiev, M., Winebrake, J. J., Johansson, L., Carr, E. W., Prank, M., Soares, J., Vira, J., Kouznetsov, R., Jalkanen, J.-P., and Corbett, J. J.: Cleaner fuels for ships provide public health benefits with climate tradeoffs, Nat. Commun., 9, 406, doi:10.1038/s41467-017-02774-9, 2018.

Song, X.-H., Hopke, P. K., Fergenson, D. P., and Prather, K. A.: Classification of Single Particles Analyzed by ATOFMS Using an Artificial Neural Network, ART-2A, Anal. Chem., 71, 860–865, doi:10.1021/ac9809682, 1999.

Sullivan, R. C., Guazzotti, S. A., Sodeman, D. A., and Prather, K. A.: Direct observations of the atmospheric processing of Asian mineral dust, Atmos. Chem. Phys., 7, 1213–1236, doi:10.5194/acp-7-1213-2007, 2007.

Sultana, C. M., Cornwell, G. C., Rodriguez, P., and Prather, K. A.: FATES: a flexible analysis toolkit for the exploration of single-particle mass spectrometer data, Atmos. Meas. Tech., 10, 1323–1334, doi:10.5194/amt-10-1323-2017, 2017.

Thomson, D. S., Middlebrook, A. M., and Murphy, D. M.: Thresholds for Laser-Induced Ion Formation from Aerosols in a Vacuum Using Ultraviolet and Vacuum-Ultraviolet Laser Wavelengths, Aerosol Sci. Technol., 26, 544–559, doi:10.1080/02786829708965452, 1997.

https://doi.org/10.5194/acp-2020-25
Preprint. Discussion started: 20 January 2020

Toner, S. M., Sodeman, D. A., and Prather, K. A.: Single Particle Characterization of Ultrafine and Accumulation Mode Particles from Heavy Duty Diesel Vehicles Using Aerosol Time-of-Flight Mass Spectrometry, Environ. Sci. Technol., 40, 3912–3921, doi:10.1021/es051455x, 2006.

Trainor, D. W. and Mani, S. A.: Pumping iron: A KrF laser pumped atomic iron laser, J. Chem. Phys., 68, 5481–5485, doi:10.1063/1.435727, 1978.

Uski, O., Jalava, P. I., Happo, M. S., Torvela, T., Leskinen, J., Mäki-Paakkanen, J., Tissari, J., Sippula, O., Lamberg, H., Jokiniemi, J., and Hirvonen, M.-R.: Effect of fuel zinc content on toxicological responses of particulate matter from pellet combustion in vitro, Sci. Total Environ., 511, 331–340, doi:10.1016/j.scitotenv.2014.12.061, 2015.

Vera, C. C., Trimborn, A., Hinz, K.-P., and Spengler, B.: Initial velocity distributions of ions generated by in-flight laser desorption/ionization of individual polystyrene latex microparticles as studied by the delayed ion extraction method, Rapid Commun. Mass Spectrom., 19, 133–146, doi:10.1002/rcm.1753, 2005.

Verdun, F. R., Krier, G., and Muller, J. F.: Increased sensitivity in laser microprobe mass analysis by using resonant two-photon ionization processes, Anal. Chem., 59, 1383–1387, doi:10.1021/ac00137a003, 1987.

Wade, E. E., Farquar, G. R., Steele, P. T., McJimpsey, E. L., Lebrilla, C. B., and Fergenson, D. P.: Wavelength and size dependence in single particle laser aerosol mass spectra, J. Aerosol Sci., 39, 657–666, doi:10.1016/j.jaerosci.2008.03.007, 2008.

Wang, G., Zhang, R., Gomez, M. E., Yang, L., Levy Zamora, M., Hu, M., Lin, Y., Peng, J., Guo, S., Meng, J., Li, J., Cheng, C., Hu, T., Ren, Y., Wang, Y., Gao, J., Cao, J., An, Z., Zhou, W., Li, G., Wang, J., Tian, P., Marrero-Ortiz, W., Secrest, J., Du, Z., Zheng, J., Shang, D., Zeng, L., Shao, M., Wang, W., Huang, Y., Wang, Y., Zhu, Y., Li, Y., Hu, J., Pan, B., Cai, L., Cheng, Y., Ji, Y., Zhang, F., Rosenfeld, D., Liss, P. S., Duce, R. A., Kolb, C. E., and Molina, M. J.: Persistent sulfate formation from London Fog to Chinese haze, Proc. Natl. Acad. Sci. USA, 113, 13630–13635, doi:10.1073/pnas.1616540113, 2016.

Woods, E., Smith, G. D., Dessiaterik, Y., Baer, T., and Miller, R. E.: Quantitative Detection of Aromatic Compounds in Single Aerosol Particle Mass Spectrometry, Anal. Chem., 73, 2317–2322, doi:10.1021/ac0011666l, 2001.

Ye, D., Klein, M., Mulholland, J. A., Russell, A. G., Weber, R., Edgerton, E. S., Chang, H. H., Sarnat, J. A., Tolbert, P. E., and Ebelt Sarnat, S.: Estimating Acute Cardiovascular Effects of Ambient PM2.5 Metals, Environ. Health Perspect., 126, 27007, doi:10.1289/EHP2182, 2018.

Young, J. P., Shaw, R. W., and Smith, D. H.: Resonance ionization mass spectrometry, Anal. Chem., 61, 1271A-1279A, doi:10.1021/ac00197a002, 1989.

Zhang, G., Bi, X., Lou, S., Li, L., Wang, H., Wang, X., Zhou, Z., Sheng, G., Fu, J., and Chen, C.: Source and mixing state of iron-containing particles in Shanghai by individual particle analysis, Chemosphere, 95, 9–16, doi:10.1016/j.chemosphere.2013.04.046, 2014.

Zhou, Y., Huang, X. H., Griffith, S. M., Li, M., Li, L., Zhou, Z., Wu, C., Meng, J., Chan, C. K., Louie, P. K.K., and Yu, J. Z.: A field measurement based scaling approach for quantification of major ions, organic carbon, and elemental carbon

https://doi.org/10.5194/acp-2020-25
Preprint. Discussion started: 20 January 2020

Atmospheric Chemistry and Physics Discussions

using a single particle aerosol mass spectrometer, Atmospheric Environ., 143, 300–312, doi:10.1016/j.atmosenv.2016.08.054, 2016.

Zimmermann, R., Ferge, T., Gälli, M., and Karlsson, R.: Application of single-particle laser desorption/ionization time-of-flight mass spectrometry for detection of polycyclic aromatic hydrocarbons from soot particles originating from an industrial combustion process, Rapid Commun. Mass Spectrom., 17, 851–859, doi:10.1002/rcm.979, 2003.